# Chapter 4
# Spider Configurations for Models with Discrete Iwan Elements

**Aabhas Singh, Mitchell Wall, Matthew S. Allen, and Robert J. Kuether**

**Abstract** Lacayo et al. (Mechanical Systems and Signal Processing, 118: 133–157, 2019) recently proposed a fast model updating approach for finite element models that include Iwan models to represent mechanical joints. The joints are defined by using RBE3 averaging constraints or RBAR rigid constraints to tie the contact surface nodes to a single node on each side, and these nodes are then connected with discrete Iwan elements to capture tangential frictional forces that contribute to the nonlinear behavior of the mechanical interfaces between bolted joints. Linear spring elements are used in the remaining directions to capture the joint stiffness. The finite element model is reduced using a Hurty/Craig-Bampton approach such that the physical interface nodes are preserved, and the Quasi-Static Modal Analysis approach is used to quickly predict the effective natural frequency and damping ratio as a function of vibration amplitude for each mode of interest. Model updating is then used to iteratively update the model such that it reproduces the correct natural frequency and damping at each amplitude level of interest. In this paper, Lacayo's updating approach is applied to the S4 Beam (Singh et al., IMAC XXXVI, 2018) giving special attention to the size and type of the multi-point constraints used to connect the structures, and their effect on the linear and nonlinear modal characteristics.

**Keywords** Iwan elements · Joints · Quasi-static modal analysis · Nonlinear updating · Model updating

## 4.1 Introduction

Mechanical structures with complicated geometry can be accurately modeled with finite element techniques if the structure is monolithic and manufactured from a single piece of material. However, even with additive manufacturing, most structures cannot be manufactured as such and therefore mechanical interfaces are introduced between sub-assemblies, which are then jointed with bolts, rivets or welds. These joints introduce uncertainty and significant modeling challenges due to the physics involved with frictional contact. While joints in general can introduce strong nonlinearity, resulting in complicated phenomena such as modal coupling, response at higher harmonics, and even chaos, in many structures of practical interest the nonlinearity is weak and is observed as a change in the effective natural frequency and damping of some of the structure's vibration modes as vibration amplitude increases.

While commercial finite element analysis or multi-body dynamics software can presumably solve contract problems with friction [1], most practitioners do not appreciate the level to which the mesh must be refined near the interface in order to obtain a predictive model. This was illustrated recently by Jewel et al. [2] who found that tens of hours were required to obtain accurate solutions for the static response of a structure with only one or two joints when the joint was meshed with adequate refinement and the solver settings were tuned to accurately solve the contact problem. It would be extremely expensive to perform dynamic simulations with such a model, and even more so for realistic structures with hundreds of joints. As a result, the majority of dynamic models use relatively coarse meshes and then spider regions of the structure to connect different parts through linear springs, whose stiffnesses can be tuned when the model is updated to correlate with test data.

In some cases, nonlinear hysteretic models are used in place of linear springs when using this whole-joint approach. These models represent the nonlinearity through constitutive equations between the degrees of freedom of a single set of

───────────────
A. Singh · M. Wall · M. S. Allen (✉)
University of Wisconsin, Madison, WI, USA
e-mail: singh36@wisc.edu; mwall4@wisc.edu; msallen@engr.wisc.edu

R. J. Kuether
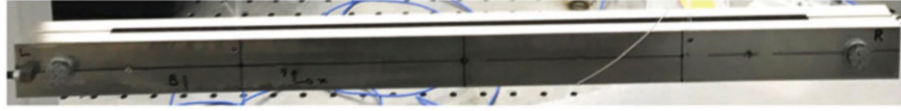Sandia National Laboratories, Albuquerque, NM, USA
e-mail: rjkueth@sandia.gov

**Fig. 4.1** The S4 Beam side view

nodes. When introduced into a reduced order model (ROM), such as a Hurty/Craig-Bampton (HCB) reduced model, they can capture nonlinear behavior while maintaining tractable computational cost. An example of the whole-joint model is the four parameter Iwan joint introduced by Segalman in 2006 [3], which was derived based on analytical solutions to contact problems and empirical data to best capture the energy dissipation observed in joints. These joint models can often be used to capture the amplitude dependent frequency or damping measured in experiments, so long as the joints remain in the micro-slip regime.

The parameters of a whole-joint model such as an Iwan element cannot currently be predicted from first principles, so measurements must be taken and model updating used to update the joint parameters until the model reproduces the measured response. The Hilbert Transform can be used to extract the frequency and damping as a function of amplitude from transient response measurements [4]. Then the recently developed Quasi-Static Modal Analysis (QSMA) approach [5, 6] can be used to quickly compute these quantities. Lacayo et al. [6] recently demonstrated this workflow to update a reduced model of the Brake-Reuss (BRB) beam. Similarly, this paper investigates the model updating procedure and applicability of the four parameter Iwan joint with a new benchmark structure studied at Sandia's Nonlinear Mechanics and Dynamics Institute in 2017 that is shown in Fig. 4.1.

The S4 Beam was studied experimentally by Singh et al. [7], and data from their study is used in this work. First, an HCB model is made for each beam and linear springs are inserted and updated to match the measured linear frequencies. Then, Iwan joints are inserted in place of some of the springs and QSMA is used to compute and iterate on the amplitude dependent damping and frequency in an effort to reproduce the experimentally measured frequency and damping. The experimental structure showed a high degree of nonlinearity in the first shearing mode (Mode 6), so the goal is to use the methodology to calibrate the model to capture this mode. In doing so, prior works have shown that a pareto front is often observed, a case in which the model cannot be updated to capture both the stiffness and damping. This work explores this issue by creating models with various types of spiders, or various ways to define the Multi-Point Constraints (MPCs) used to reduce the contact surfaces to a single node.

## 4.2 Modeling Approach

### 4.2.1 Hurty/Craig Bampton Reduction

To incorporate the high geometric detail of the structures of interest, finite element models can quickly become excessively large and computationally expensive. As a result, ROMs are used to approximate the full-order model at a set of reduction nodes between the mechanical interfaces. The approximation requires that these components remain linear and that the only source of nonlinearity within in the joined system is at the contact interface [8]. Although many methods of model reduction exist, this paper will focus on the HCB method as discussed in [9]. The FE discretized equations of motion for an undamped multi-degree of freedom (MDOF) system are given by Eq. 4.1, where $\mathbf{M}$ is the mass matrix, $\mathbf{K}$ is the stiffness matrix, $\mathbf{F}$ is the external forcing, $\mathbf{F}_J(\mathbf{u})$ is the joint force (either linear or nonlinear) and $\mathbf{u}$ is the physical displacement.

$$\mathbf{M}\ddot{\mathbf{u}} + \mathbf{K}\mathbf{u} + \mathbf{F}_J(\mathbf{u}) = \mathbf{F} \tag{4.1}$$

The system can be equivalently written with matrices partitioned between the boundary and interface DOFs as

$$\begin{bmatrix} \mathbf{M}_{ii} & \mathbf{M}_{ib} \\ \mathbf{M}_{bi} & \mathbf{M}_{bb} \end{bmatrix} \begin{Bmatrix} \ddot{\mathbf{u}}_i \\ \ddot{\mathbf{u}}_b \end{Bmatrix} + \begin{bmatrix} \mathbf{K}_{ii} & \mathbf{K}_{ib} \\ \mathbf{K}_{bi} & \mathbf{K}_{bb} \end{bmatrix} \begin{Bmatrix} \mathbf{u}_i \\ \mathbf{u}_b \end{Bmatrix} + \begin{Bmatrix} 0 \\ \mathbf{F}_{J,b}(\mathbf{u}_b) \end{Bmatrix} = \begin{Bmatrix} 0 \\ \mathbf{F}_b \end{Bmatrix} \tag{4.2}$$

where subscripts $b$ and $i$ represent the boundary and interface DOF respectively. Note that only the boundary DOF are assumed to be forced either externally or internally through the joint. Then, a small number of fixed interface modes,[1] $\Phi$, are

---

[1]Fixed interface modes are normal modes obtained by fixing the interface between two subcomponents.

computed and that basis is augmented with constraint modes,[2] $\boldsymbol{\Psi}$, as detailed [10] to obtain the HCB transformation matrix in Eq. 4.3.

$$\begin{Bmatrix} \mathbf{u}_i \\ \mathbf{u}_b \end{Bmatrix} = \mathbf{T}^{HCB} \begin{Bmatrix} \mathbf{q}_k \\ \mathbf{u}_b \end{Bmatrix} = \begin{bmatrix} \boldsymbol{\Phi} & \boldsymbol{\Psi} \\ \mathbf{0} & \mathbf{I} \end{bmatrix} \begin{Bmatrix} \mathbf{q}_k \\ \mathbf{u}_b \end{Bmatrix} \tag{4.3}$$

This transformation then reduces the equations of motion to those shown in Eq. 4.4.

$$\left(\mathbf{T}^{HCB}\right)^{\mathrm{T}} \begin{bmatrix} \mathbf{M}_{ii} & \mathbf{M}_{ib} \\ \mathbf{M}_{bi} & \mathbf{M}_{bb} \end{bmatrix} \mathbf{T}^{HCB} \begin{Bmatrix} \ddot{\mathbf{q}}_k \\ \ddot{\mathbf{u}}_b \end{Bmatrix} + \left(\mathbf{T}^{HCB}\right)^{\mathrm{T}} \begin{bmatrix} \mathbf{K}_{ii} & \mathbf{K}_{ib} \\ \mathbf{K}_{bi} & \mathbf{K}_{bb} \end{bmatrix} \mathbf{T}^{HCB} \begin{Bmatrix} \mathbf{q}_k \\ \mathbf{u}_b \end{Bmatrix} + \begin{Bmatrix} \mathbf{0} \\ \mathbf{F}_{J,b}\left(\mathbf{u}_b\right) \end{Bmatrix} = \begin{Bmatrix} \mathbf{0} \\ \mathbf{F}_b \end{Bmatrix} \tag{4.4}$$

The ROM can be used to analyze the dynamic response of a structure more efficiently than a dynamic simulation of a full finite element model.

### 4.2.2  Spidering

In order to connect the contact surfaces with one-dimensional linear or nonlinear elements, two types of spider elements were used in this work, which shall be referred to as RBAR and RBE3 elements (i.e. using NASTRAN's naming convention). An RBAR element is a rigid beam that rigidly constrains each node to a single node with 6 DOF, whereas an RBE3 is an averaging element that ties the average displacement and rotation of the surface to that of the slave node [11]. Both are types of MPCs (Fig. 4.2). Depicts an example of the MPC spiders on the S4B. Note that separate virtual and HCB reduction nodes had to be created because the implementation of the HCB method within Sandia National Laboratories Sierra Structural Dynamics (Sierra/SD) code doesn't allow a virtual node to be used as an interface node in a HCB model [11]. These are shown expanded for visualization, but in fact they are all concident.

The spiders reduce an area of nodes to a single point that can be used to connect the surfaces. These spiders can be used to attach linear springs or Iwan elements to capture the linear/nonlinear dynamics of the system.

### 4.2.3  Whole-Joint Model

One of the most well-developed whole-joint models is Segalman's 4-parameter Iwan element. It was developed as part of a large research effort at Sandia National Laboratories that considered both analytical solutions for contact and empirical evidence that showed that joints exhibit power-law energy dissipation versus force (or vibration amplitude) [3]. An Iwan

**Fig. 4.2** Finite element model of the S4B depicting the CS



CB Reduction Nodes

"Virtual" Nodes

RBAR/RBE3 Elements

---
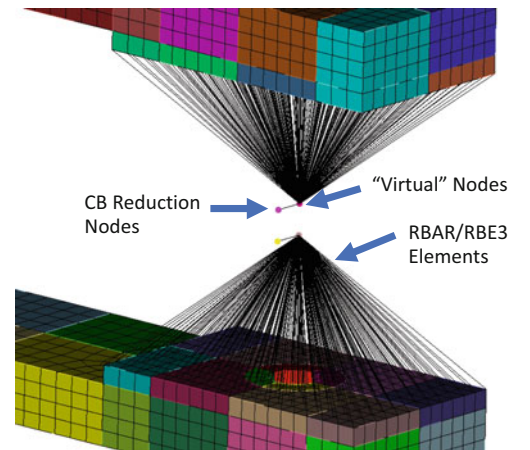
[2]Constraint modes are obtained by deflecting a single mode by a unit displacement while fixing the other DOF.

**Table 4.1** Definition of Iwan parameters (physical description)

| | |
|---|---|
| $F_s$ | The force necessary to cause macroslip |
| $K_T$ | The tangential stiffness of the Jenkins elements (i.e. the joint stiffness when no slip occurs) |
| $\chi$ | The exponent that describes the slope of the energy dissipation curve |
| $\beta$ | The ratio of the number of Jenkins elements that slip before micro-slip and then at macroslip |

element is simply a collection of slider or Jenkins elements in parallel, in which the slip force[3] for each slider is chosen to create an element that exhibits power-law energy dissipation. This approach simplifies joint modeling significantly; typical joint models consider every point in the interface to be independent and goverened by several parameters, i.e. the friction coefficient, normal force, etc. . . . When one multiplies these unknowns by the number of contact elements there may be hundreds or thousands of free parameters. Segalman's model recognizes that the net effect of all of these parameters must be to produce power-law dissipation versus vibration amplitude, which is goverened by only two of the four parameters in the Iwan model. The other two parameters control the transition to macro-slip when the joint slips completely. Macro-slip is typically not observed in engineered joints if they are tightened properly, except perhaps under extreme loading.

The four parameter Iwan model can be represented by four parameters: $F_s$, $K_T$, $\chi$, and $\beta$, given in Table 4.1. For an in-depth discussion of the Iwan element, refer to [3].

For the nonlinear analysis, the Iwan joint replaces a linear spring between two spiders, and the corresponding spring constant becomes the $K_T$ parameter of the Iwan element.

### 4.2.4 Linear Model Updating

Between the single point reduced interfaces, six DOF springs are attached to calibrate the linear natural frequencies of the model to the experimental data. Linear springs are attached with three translational and three rotational spring constants. These constants were varied from 1e4 to 1e10 (lb/in or in-lb/rad) in a Monte Carlo study to minimize the difference between the model and experimental frequencies as shown in Eq. 4.5.

$$Objective\ Function = \sum_{i=1}^{n} \left( \frac{\omega_{\text{model},i} - \omega_{\text{test},i}}{\omega_{\text{test},i}} \right)^2 \tag{4.5}$$

The results of the Monte Carlo updating are presented in Sects. 4.3 and 4.4.

### 4.2.5 Nonlinear Model Updating

Quasi-Static Modal Analysis (QSMA) was originally proposed by Festjens et al. [5] as a method that replaces a dynamic simulation of a joint with a quasi-static problem that can be solved to estimate the effective natural frequency and damping of a single mode due to the joints in the structure. A quasi-static distributed force is applied that replicates the inertial loading experienced during vibration in that mode and coupling between the vibration modes is ignored. Lacayo and Allen further extended QSMA, developing an even faster algorithm for the case where the joints are represented by Iwan elements [14]. The theory is presented in depth in that paper and for brevity it will not be repeated here other than key points. The HCB model still has the general form given in Eq. 4.1, and the nonlinear joints can be represented through a nonlinear force $\mathbf{F}_J(\mathbf{u})$ as shown in Eq. 4.6.

$$\mathbf{M}\ddot{u} + \mathbf{K}u + \mathbf{F}_J(\mathbf{u}) = \mathbf{F} \tag{4.6}$$

QSMA consists of solving the equation above for a static case, i.e. $\ddot{u} = 0$, where the forcing is $\mathbf{F} = \alpha[\mathbf{M}]\varphi_i$. After solving Eq. 4.6, one obtains the static response, $\mathbf{u}(\alpha)$, from which the modal velocity amplitude, natural frequency, and damping ratio can be written as function of $\alpha$ as shown in Eqs. 12–17 in [14]. The damping ratio is obtained from a load-displacement

---

[3]If all sliders have the same friction coefficient then the slip force is defined by the normal force for each slider.

hysteresis curve that is derived using Masing's Rules. Given that all three variables are functions of amplitude, the damping and natural frequency can be plotted in terms of modal velocity amplitude and this is the convention that will be used in this work.

## 4.3    Application to S4 Beam: Linear Updating

The finite element model used for the S4 Beam is shown in Fig. 4.3. This high-fidelity model incorporates two C shaped beams that are held together by bolts. The bolts were modeled separately and glued to the top and bottom of the beam, but with the contact interfaces between the beams left free to slide relative to each other or to penetrate.

Prior to adding the linear springs or nonlinear Iwan elements, the FEM was reduced by creating a HCB model in which only the spider DOF were retained as interface nodes to create a compact and efficient model for the linear and nonlinear structure. The resulting model had 24 interface DOF (a six DOF virtual node at each of the four interfaces) and 30 fixed interface modes. This reduced the FEM to 54 DOF. The output transfer matrices were saved so that the response could be computed at 22 observation nodes, which were spaced every 2.5″ along the top and bottom of the beam.

For this paper, the spiders were defined over two different areas: the full interface and a reduced interface, both of which are shown in Fig. 4.4. The full interface consists of all nodes on the flat portion where contact is possible whereas the reduced interface consists of nodes that were found to be in contact in a nonlinear contact simulation that was performed in Abaqus. The result of this contact simulation is also shown in Fig. 4.4. Note that this simulation approximates the surfaces as perfectly smooth and flat, and there is some evidence, as reported in [7], that the surfaces were not truly flat. Nevertheless, these models are in line with the typical approach, considering the information that might be available during the design of a structure. For each of the interface areas, two models were created, one using RBAR elements and one using RBE3s, resulting in a total of four candidate HCB models.
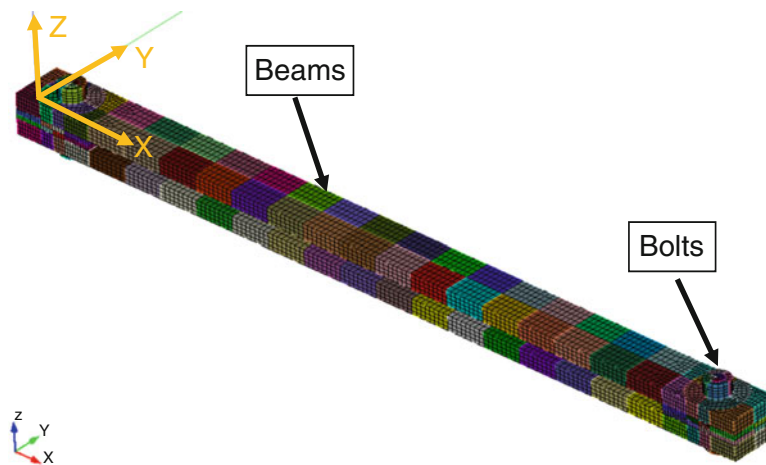


**Fig. 4.3** Finite element model of the S4B depicting the coordinate system. The beam is segmented into blocks with nodes corresponding to measurement points
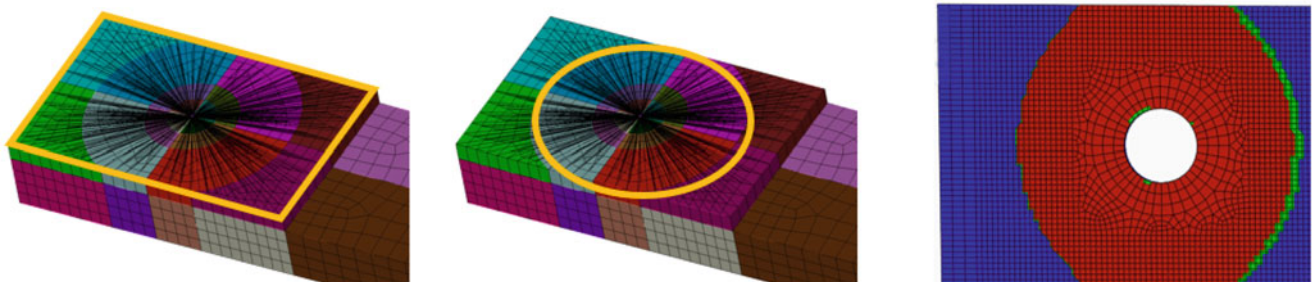


**Fig. 4.4** (Left) Full contact area, (Middle) Reduced contact area, (Right) Abaqus Contact Simulation

**Table 4.2** Modes of a single beam (half of the S4 assembly) vs. model frequencies

| Mode | Description | Experimental frequency (Hz) | Single beam model frequency (Hz) | Percent error (%) |
|---|---|---|---|---|
| 1 | 1st Bending | 177.87 | 177.29 | −0.33 |
| 2 | 2nd Bending | 497.84 | 498.09 | 0.05 |
| 3 | 1st Stiff Bending | 576.00 | 576.84 | 0.14 |
| 4 | 2nd Stiff Bending | 979.84 | 988.44 | 0.88 |
| 5 | Torsion | 1474.67 | 1471.22 | −0.23 |
| 6 | – | 1556.46 | – | – |
| 7 | Torsion | 1585.58 | 1595.47 | 0.62 |

**Table 4.3** Single beam material property updating

| | Nominal | Optimal |
|---|---|---|
| Elastic Modulus | 29,000 (ksi) | 27,245 (ksi) (−6.05%) |
| Poisson Ratio | 0.29 | 0.29 (0.00%) |

### 4.3.1  Single Beam Calibration

Prior to calibrating the whole-joint models with linear springs, a finite element model for a single beam was used to calibrate the material properties for steel. Table 4.2 lists the adjusted elastic modulus and Poisson ratio for the single beam and shows the resulting agreement between the experimental natural frequencies and those of the model. All model frequencies were within 1% of the experimental frequencies, with the highest error in a second stiff bending mode. The densities of the model were calibrated by measuring the mass of the experimental beams and dividing by the volume of the FEM to ensure that the FEM has correct mass. The first four elastic bending modes were used to tune the elastic modulus and the fifth and seventh modes (torsion) were used to tune the Poisson ratio. Although, Mode 6 for the single beam was identified by the experimental setup, it was not matched within the FEM and thus was not used in the calibration of the beam. These properties were then used in all subsequent modeling (Table 4.3).

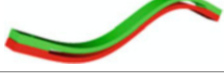### 4.3.2  Whole-Joint Spring Calibration

Linear model updating was performed for all four candidate models, and after using a Monte Carlo Simulation to minimize the objective function in Eq. 4.5, a set of values was found for each of the six spring constants. The springs on either end of the S4 beam were assumed to be identical. Tables 4.4 and 4.5 depict the percent error natural frequencies of the assembly after optimization and the spring stiffnesses for each of the cases respectively.

The S4 Beam has several different types of mode shapes, and each is influenced by different springs depending on how the joint is loaded. The mode shapes shown in Table 4.4 can be used to deduce these differences. For example, Modes 1 and 5 involve opening of the joint and hence are most sensitive to the Z-direction translational stiffness, whereas Mode 4 is completely insensitive to the joint stiffness.

While the overall agreement was similar for each candidate model, a few differences are noted between the results obtained using RBE3 and RBAR elements. Most notably, the models with RBE3s were not able to capture Mode 2 as accurately; this mode is sensitive to the axial stiffness of the joint, loading it in the fashion of the lap joints that have been studied in many prior works [6, 12]. The RBE3 models have very high values for $T_x$ and yet they still under-predict the frequency of this mode. On the other hand, the RBE3 models do slightly better at predicting the frequencies of Mode 1, and this might have been expected since the RBE3 doesn't artificially rigidize the interface and Mode 1 would tend to be sensitive to this because it bends the interface region.

In comparing the results with the reduced and full interfaces, one can see that the reduced interface typically required higher spring stiffnesses than the full interface (e.g. consider $R_Y$ in Table 4.5). This result makes sense, as reducing the interface area effectively decreases the stiffness of the joint region, and so the spring constants must be increased to compensate. To get a sense of how sensitive the natural frequencies are to the spring constants found in each case, the constants for the full interface RBAR case were used in the three other models and the natural frequencies were computed. As expected, the natural frequencies of modes 3 and 4 didn't change significantly. However, the models gave frequency errors ranging from 1 to 7% for the other modes. For conciseness, these results are presented in the Appendix.

**Table 4.4** Natural frequency errors for each of the candidate models

| Mode # | Test [Hz] | Full interface RBAR (%) | Full interface RBE3 (%) | Reduced interface RBAR (%) | Reduced interface RBE3 (%) | Reduced, bonded interface (%) | Mode shape |
|---|---|---|---|---|---|---|---|
| 1 | 258.0 | 0.60 | 0.43 | 0.63 | 0.29 | 3.65 | |
| 2 | 331.7 | 0.37 | −1.65 | −0.47 | −2.12 | −0.48 | |
| 3 | 478.6 | −0.78 | −0.98 | −0.87 | −0.99 | −0.88 | |
| 4 | 567.7 | −2.20 | −2.24 | −2.22 | −2.23 | −2.25 | |
| 5 | 708.3 | −0.78 | −0.05 | −0.25 | −0.12 | 3.71 | |
| 6 | 851.5 | −0.34 | 0.33 | 0.16 | 0.12 | 4.26 | |

The four candidate models contain different spider areas (full vs. reduced) and different constraint elements (RBAR vs. RBE3)

**Table 4.5** Linear spring stiffnesses for each candidate model

| Spring | Full interface *RBAR* spring | Full interface *RBE3* spring | Reduced interface *RBAR* spring | Reduced interface *RBE3* spring |
|---|---|---|---|---|
| $T_X$ [**lb/in**] | 1.00E+08 | 1.65E+10 | 6.71E+12 | 5.04E+11 |
| $T_Y$ [**lb/in**] | 1.43E+12 | 1.68E+05 | 1.20E+05 | 1.43E+09 |
| $T_Z$ [**lb/in**] | 4.61E+03 | 1.64E+02 | 1.48E+03 | 3.00E+04 |
| $R_X \left[ \frac{\text{in-lb}}{\text{rad}} \right]$ | 2.55E+07 | 8.59E+04 | 1.25E+06 | 2.85E+06 |
| $R_Y \left[ \frac{\text{in-lb}}{\text{rad}} \right]$ | 3.66E+05 | 1.89E+06 | 6.10E+05 | 1.04E+07 |
| $R_Z \left[ \frac{\text{in-lb}}{\text{rad}} \right]$ | 2.08E+06 | 7.72E+11 | 4.15E+07 | 1.82E+07 |

In the end, considering only the ability of the models to capture the linear natural frequencies, the best models contained RBAR elements, as those were able to best capture Mode 2. Overall, the area of influence had a weaker effect than the choice of spider elements (i.e. RBAR vs. RBE3). These effects are somewhat overshadowed by the errors in Modes 3 and 4, which were not sensitive to any spring constants. All modes, apart from Mode 4, were correlated to below one percent error. Mode 4 is the only mode that involves bending in the y-direction (stiff direction), and the six springs all have negligible effect on this mode since the joint is not loaded when the structure bends into this mode. It was thought that this mode may be sensitive to the mass of the bolts or accelerometers, but those were included in the model and their values verified and even then, the agreement shown is the best that could be obtained within the timeline of the project. Furthermore, since this mode is linear, this mode was not one of interest and no further steps were taken to improve correlation and as a result, these spring stiffnesses can be then applied as a basis for QSMA.

The uncertainty of these spring parameters must be evaluated prior to nonlinear updating, i.e. can different sets of parameters produce the same linear natural frequencies? If so, there is additional uncertainty and these parameters must be variable during nonlinear updating. Figure 4.5 shows the objective function for each iteration of the Monte Carlo study versus each of the spring stiffnesses.

This figure illustrates that the objective function, and hence the percent error in each natural frequency, is governed primarily by the Y rotation spring stiffness. The objective function can be small even when the other spring stiffnesses vary by several orders of magnitude, but it is only small if Y is between about 2e5 and 8e5 in-lb/rad. In other words, there are no other local minima that might produce similar results. Additionally, the X translation spring and the Z rotation spring must be above about $10^6$ in order to obtain good correlation. To further illustrate which parameters are important in linear updating
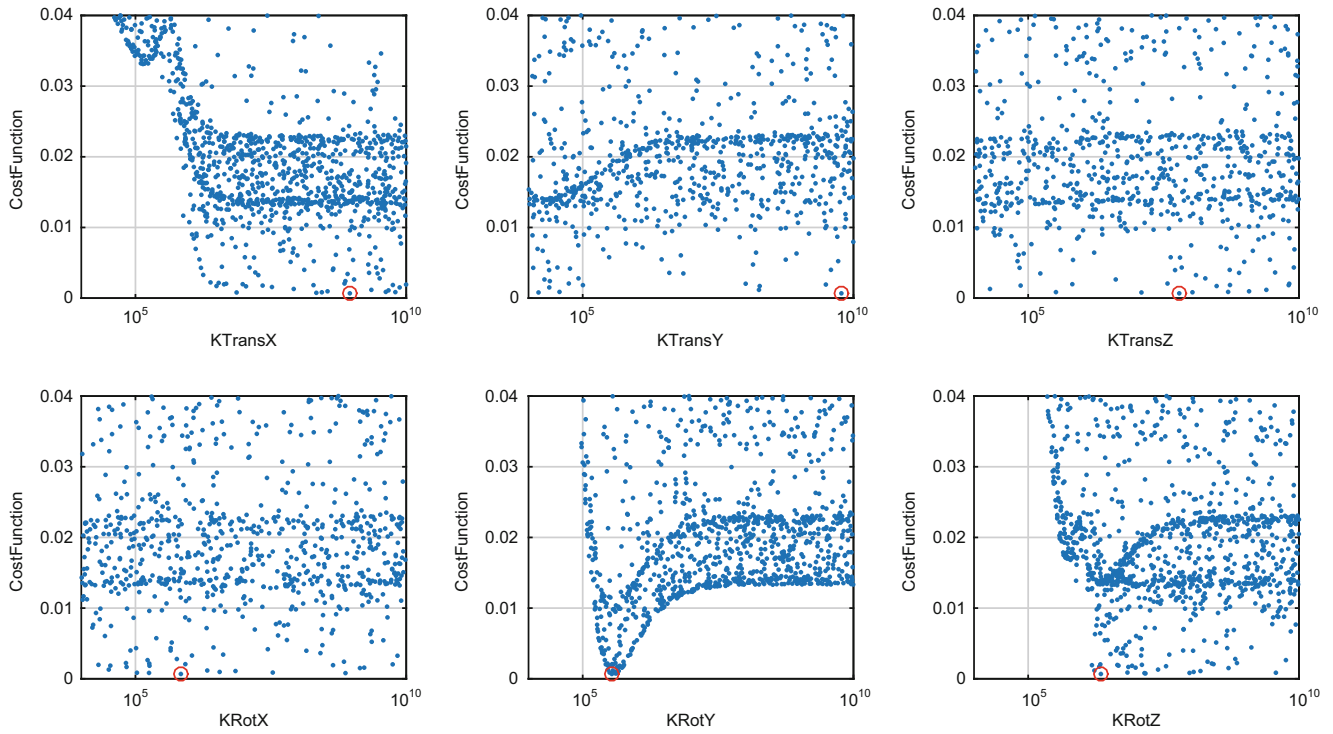
**Fig. 4.5** Monte Carlo study depicting the objective function as a function of the spring stiffnesses for the Full Interface RBAR model
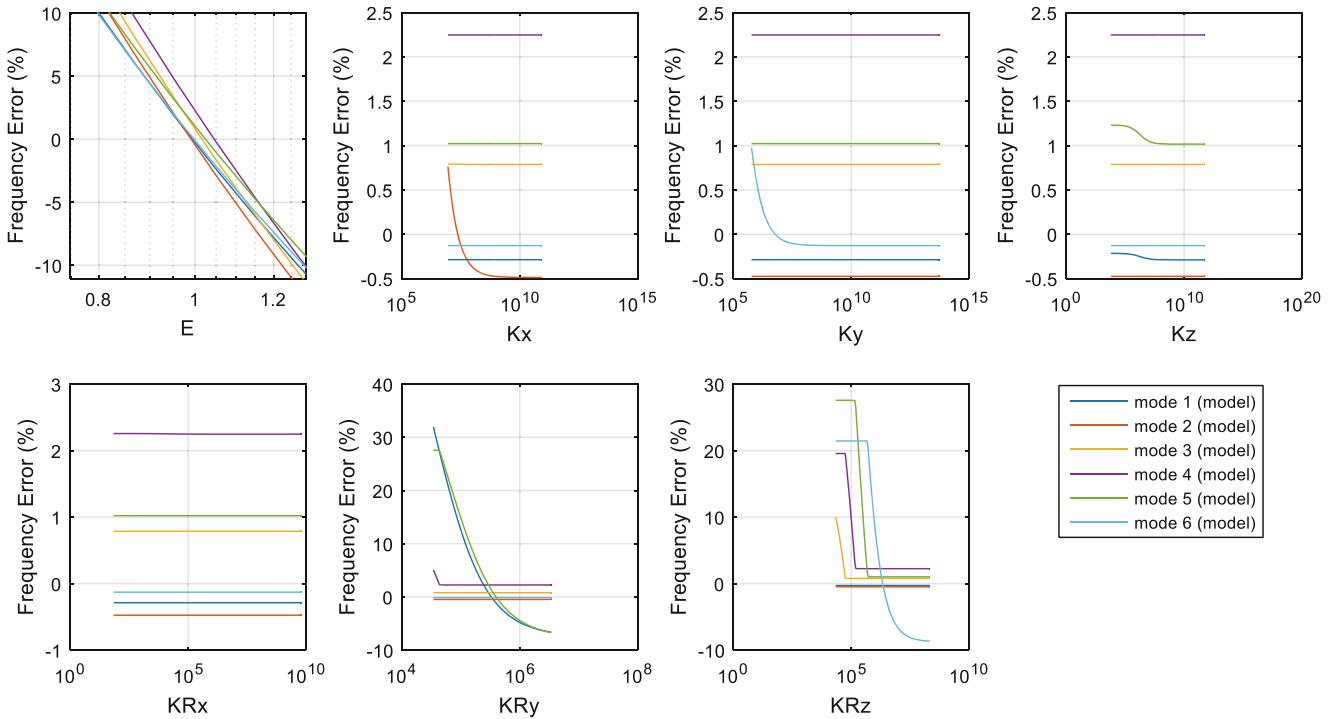


**Fig. 4.6** Frequency Error as each spring stiffness is varied separately for the full interface RBAR model

and what ranges for these parameters might be reasonable, Fig. 4.6 depicts the percent error in each natural frequency (compared to the experimental) as each design variable changes relative to the values in Table 4.5.

Although the elastic modulus was established with the single beam study, it was varied in the parameter study to see if the second beam affected the modulus of the system. It changes the frequencies of every mode in approximately the same

way. Furthermore, no value of the X rotation spring stiffness can better correlate the model since the joints and modes do not exercise this rotation within the frequency range of interest. For the other parameters, there exists an optimal value that can improve the correlation of some modes, while not affecting the other modes. Mode 2 is only sensitive to X translation spring stiffness but has a large range of applicable values that result in little change in the other linear frequencies. This allows the freedom to vary the parameter in nonlinear updating in order to improve correlation. For Mode 6, a mode involving shearing of the joint, the Y translation and Z rotation springs can be selected to minimize the error, while marginally affecting the other modes. However, there is little freedom to vary the Z rotation spring stiffness before one begins to reduce the correlation of the fifth and sixth natural frequencies.

## 4.4 Nonlinear Model Updating

This paper uses the methodology discussed in Sect. 4.2 to identify the Iwan parameters of the whole-joints. In the results that follow, since only Mode 6 was considered, an Iwan element was only placed in the Z rotation direction since that affects the shearing of the joint and is assumed to cause the nonlinearity observed in this mode. The tangential stiffness ($K_t$) of the joint is chosen as the linear stiffness obtained from the linear model updating, while the other three parameters are free parameters to be calibrated. In order to ensure that a global optimum is obtained, Monte Carlo simulation (MCS) is used to explore the parameter space and find an optimal solution for unknown Iwan parameters. Before running MCS, it is informative to first perform a sweep of some of the parameters to understand what effect they have and to define limits over which to vary the parameters in the MCS. The power law exponent, $\chi$, is measured from the slope of the experimental damping vs. amplitude curve [3, 13], and therefore is treated as a known parameter in this study; however since $F_s$ and $\beta$ cannot be measured, they are allowed to vary. To illustrate the effect of these parameters, using $\chi = -0.12$ and an arbitrary $\beta = 1$ for both of the joints (in the z-rotation direction), and allowing $F_s$ to vary over a large range, we see the behavior shown in Fig. 4.7. The model predictions are compared with the measurement for Mode 6 at an impact level of 22.5 lbf and a torque levels of 25.1 N-m (18.5 ft-lb).

This preliminary test shows excellent correlation between model and experiment for both damping and frequency trends for $F_s = 0.599$, and gives an idea of how large of a change in $F_s$ might be needed to probe the parameter space. This was repeated for various values of $\beta$, revealing that $\beta$ had a much weaker effect. This provided an initial guess for $F_s$ and established the range of these parameters to use in the Monte Carlo simulation.
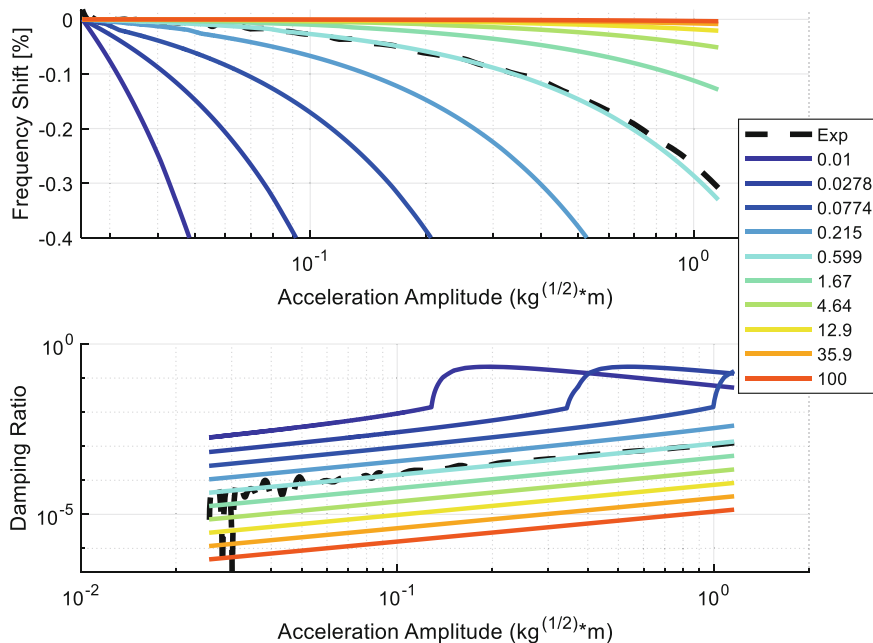


**Fig. 4.7** Frequency shift and Damping ratio amplitude dependency for different **F$_s$** values for the full interface RBAR model
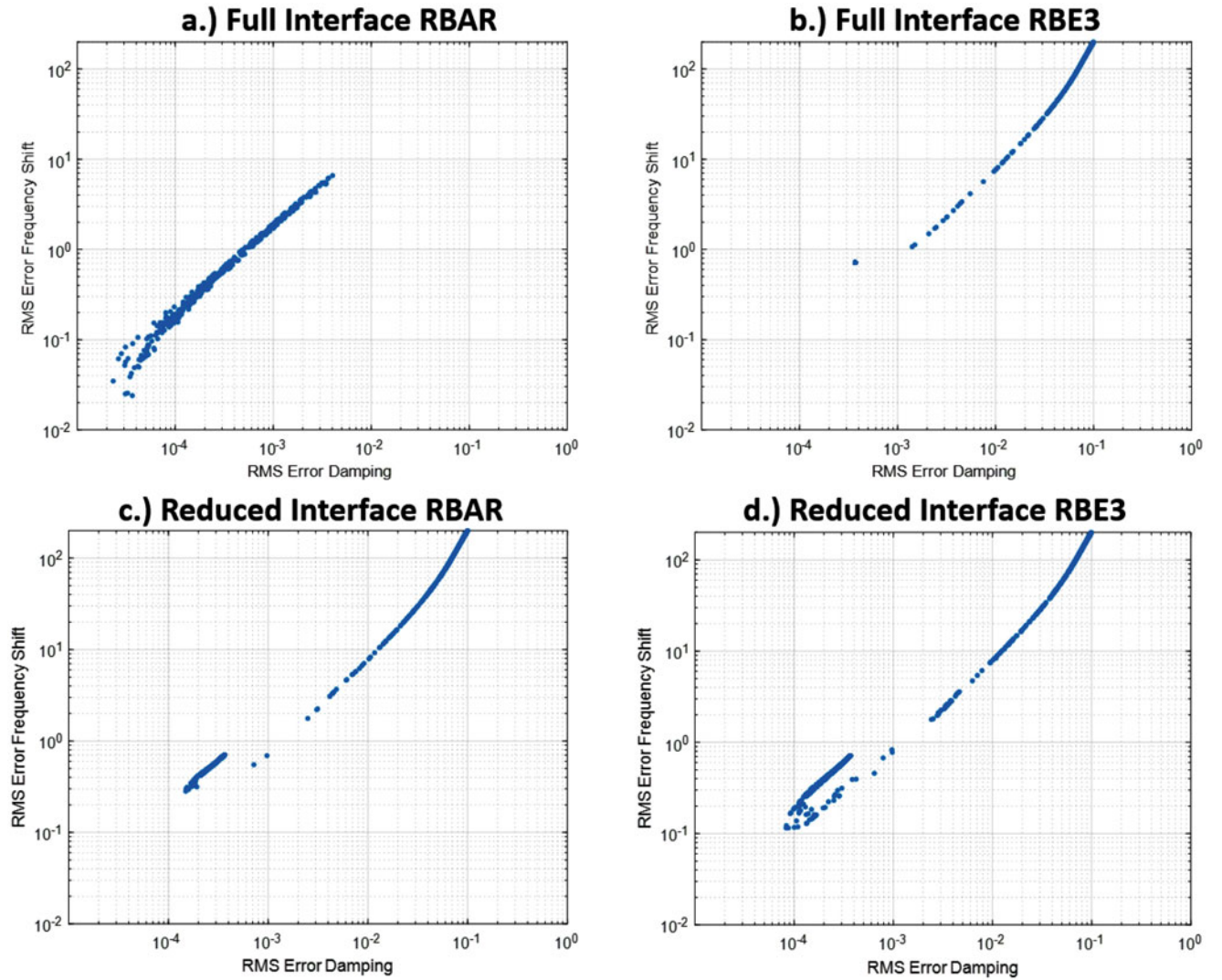
**Fig. 4.8** RMS error for frequency shift and damping for the Monte Carlo simulations with (**a**) Full Interface RBAR, (**b**) Full Interface RBE3, (**c**) Reduced Interface RBAR, and (**d**) Reduced Interface RBE3 models

**Table 4.6** Iwan parameters and errors from the Monte Carlo simulations

| Interface | $F_s$ | $K_t$ | $\chi$ | $\beta$ | RMS $\omega_n$ shift error (Hz) | RMS damping error |
|---|---|---|---|---|---|---|
| Full RBAR | 0.4472 | 2.08e6 | −0.1697 | 2.3521 | 0.023 | 2.62e−5 |
| Reduced RBAR | 0.0971 | 4.15e7 | −0.1833 | 7.589e-5 | 0.274 | 1.567e−4 |
| Full RBE3 | 0.0945 | 7.72e11 | −0.112 | 0.00307 | 0.716 | 3.6975e−4 |
| Reduced RBE3 | 0.1207 | 1.83e7 | −0.1905 | 0.000951 | 0.113 | 1.155e−4 |

A large Monte Carlo simulation was then conducted for full/reduced interfaces and RBAR/RBE3 joint models where $\beta$ was uniformly distributed in a logarithmic sense over 6 orders of magnitude, centered on $\beta = 0.1$, and $F_s$ as well over 2 orders of magnitude centered on $F_s = 0.1$, while $\chi$ was varied linearly between 0 and −0.2. Figure 4.8 depicts the root mean square (RMS) error in damping and frequency shift for each iteration of the MCS, and Table 4.6 gives the numerical value of the RMS errors and the Iwan parameters obtained for the optimal solution.

In the study in [14] a Pareto front was observed where one was forced to choose between low error in frequency or damping. In contrast, in this study the RMS error in frequency and damping are found to tend to zero together. However, the minimum errors obtained in each model vary quite significantly, with the Full Interface RBAR model obtaining an order of magnitude smaller error in frequency and damping than the others (see Table 4.6). Furthermore, the maximum errors varied greatly for each of the models, with the Full RBAR model having the least maximum RMS error in both frequency and
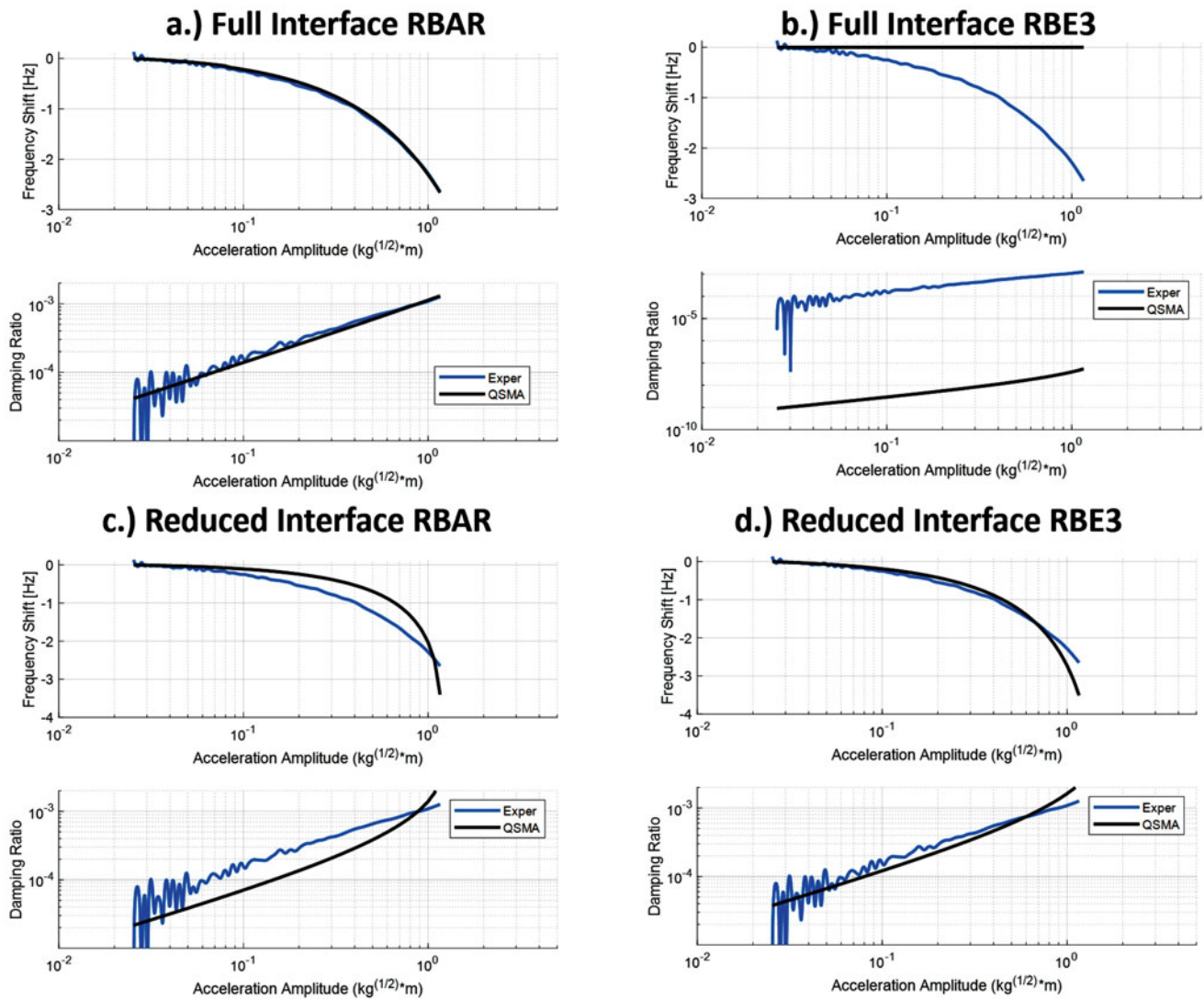
**Fig. 4.9** Experimental damping and frequency shift versus QSMA predictions for the candidate models after optimization for (**a**) Full Interface RBAR, (**b**) Full Interface RBE3, (**c**) Reduced Interface RBAR, and (**d**) Reduced Interface RBE3 models

damping. So, in a sense, each of these models is limited in how well it can fit the measurements for any value of the Iwan parameters, as was the model in [6].

The amplitude dependent frequency and damping for each set of optimal Iwan parameters are shown in Fig. 4.9, where the best solution is obtained by the Full Interface RBAR model and the Full Interface RBE3 model gave very poor results. The optimization routine was able to find reasonably good correlation for the other two models, however, the curve in the damping vs. amplitude plots reveals that the parameters of the Iwan joints are tuned such that the models are nearing macro-slip. As a result, the models do not agree very well at higher amplitudes, and if the model was forced a little too high then it might exhibit macro-slip whereas the measurements show no sign that macro-slip is imminent. Interestingly, this same behavior was observed in the study by Lacayo et al. [6], and was the primary deficiency in their reduced model. The authors have had similar experiences with other models.

In an effort to understand why the Full Interface RBAR model was superior, a parameter study was conducted in the spring stiffness was varied for the Full Interface RBAR model and the resulting frequency and damping curves are shown in Fig. 4.10. In this case study, the optimal $F_s$, $\chi$ and $\beta$ values were used, and the spring stiffness was varied from 1 to 10,000% of the value obtained from linear updating. This parameter study shows that a small decrease in $K_t$ leads to an increase in damping. However, as $K_t$ is decreased further, the damping begins to decrease. In other words, there is not a single, simple
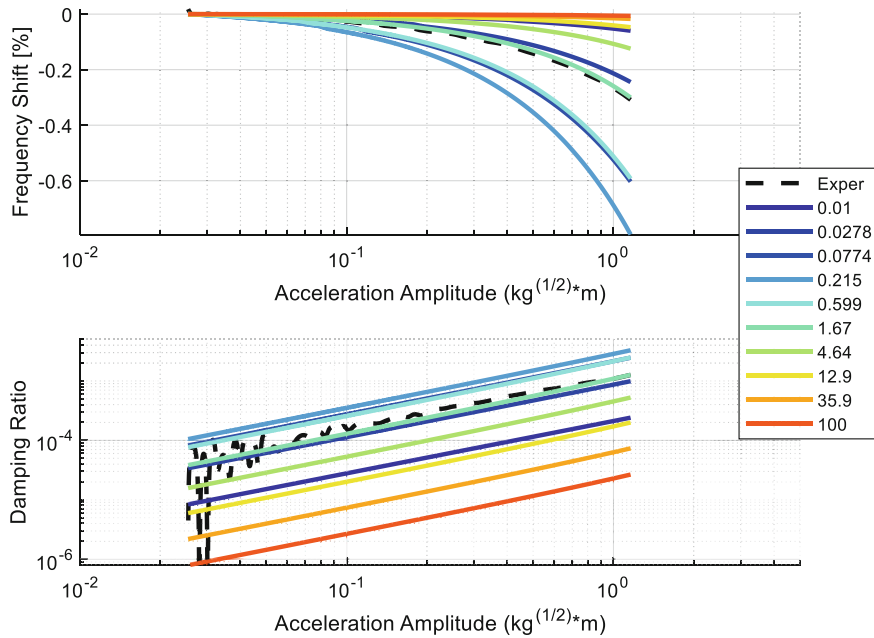
**Fig. 4.10** Natural frequency and damping versus amplitude when the Iwan joint stiffness ($K_t$) is scaled and varied with the other parameters held at their optimal values for the Full Interface RBAR model
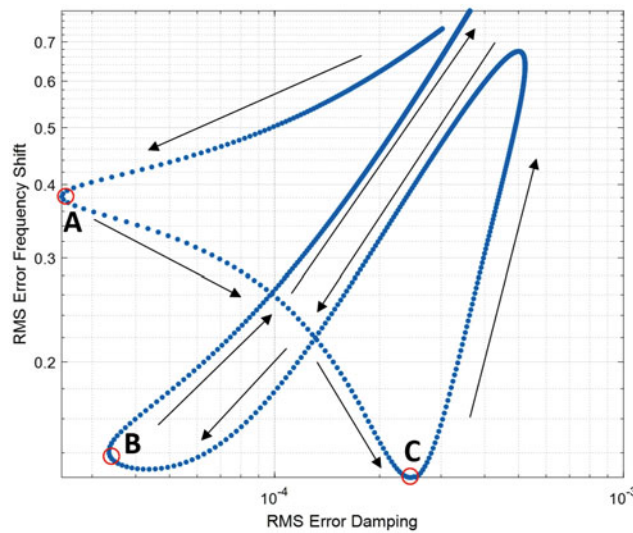


**Fig. 4.11** Error plot for the case study where the Iwan joint stiffness ($K_t$) is varied and $F_s$ is held at the optimal value for the Full Interface RBAR model

rule of thumb governing how $K_t$ will affect the results. To explore this further, QSMA was performed for 1000 values of $K_t$ between 1 and 10,000% and the RMS Error in frequency and damping is shown in Fig. 4.11.

The results in Fig. 4.11 further show that the frequency shift and damping do not depend monotonically on $K_t$, and that one might observe several Pareto fronts, depending on the range used for $K_t$. The arrows show the direction of increasing stiffness. A solution in Region A will yield only excellent damping correlation, whereas a solution in region B will yield only excellent frequency correlation. Region B will yield the optimal solution for both damping and frequency. Clearly the quasi-static solution depends strongly on $K_t$, and yet, for a single spidering method one has little leeway in adjusting the value of $K_t$, without impairing the model's ability to capture the linear natural frequencies of the structure. Furthermore, this case study was conducted with an $F_s$ value that correlates to an optimal solution using the nominal $K_t$, and different results might be obtained for other values of $F_s$.

It is very interesting that, although these models all produced relatively similar results for linear updating, they produce completely different results for the nonlinear damping. Furthermore, since the reduced interface of the S4B was established through a nonlinear contact simulation, it was expected that the reduced interface would yield the most optimal results; however, this was not the case as the full interface was most accurately able to capture the measured dynamic behavior.

## 4.5  Conclusion

This paper explored the applicability of linear and nonlinear model updating to a new nonlinear benchmark structure, the S4 Beam. High fidelity models were created using RBAR and RBE3 spidered joints to understand the effects of the area of influence for the joint (i.e. using full and reduced contact interface areas). The viability of the models was studied by evaluating their ability to reproduce the linear natural frequencies of the assembly (i.e. by updating linear springs at the interface) and their ability to capture the amplitude dependent frequency and damping caused by the joints (i.e. by updating the parameters of nonlinear Iwan elements at the interfaces).

The linear updating exercise showed that all models were quite similar, although the models with spiders constructed with rigid bar elements captured the second mode more accurately, and this was significant because the second mode was sensitive to shearing of the joint due to bending of the beam, a phenomenon that is often observed in lap joints. We also explored simply bonding all nodes in the interface that were found to be in contact by a high fidelity simulation of preload, but we did not obtain as good of agreement using that approach as was seen by Fronk et al. [14] although that aspect of this study deserves further investigation.

Quasi-static modal analysis was then used to update the parameters of the nonlinear Iwan elements, using the joint stiffnesses found in the linear updating step. Although the models captured the linear modes quite similarly, they produced a widely varying results for the nonlinear damping and for the change in frequency with vibration amplitude. The model with a full interface spidered with RBAR elements resulted in the excellent correlation between the experimental nonlinear frequency and damping curves, perhaps the best that has been observed in this type of study to date, whereas the model that used the Full Interface with RBE3 spiders gave very poor results. Both of the models using a reduced interface area gave reasonable correlation, but the Iwan joints were forced to the verge of macro-slip and so one would not have high confidence in simulations from these models. The preliminary conclusion of this work is that the method of spidering the interface does indeed matter very much for this type of modeling. Future work will be needed to understand this further and to develop best practices.

## Appendix: Full Interface RBAR Springs for all Models

In this case study, the full interface RBAR case linear spring stiffnesses were used to attach the four interfaces for the other three models. The tables below depict their results with Table 4.7 showing the linear frequencies and Table 4.8 showing the percent errors.

**Table 4.7**  Linear frequencies for each model using the spring stiffnesses of the full interface RBAR case

| Mode # | Experimental (Hz) | Full interface RBAR (Hz) | Full interface RBE3 (Hz) | Reduced interface RBAR (Hz) | Reduced interface RBE3 (Hz) |
|---|---|---|---|---|---|
| 1 | 258.01 | 259.56 | 246.92 | 253.41 | 244.39 |
| 2 | 331.73 | 332.97 | 325.90 | 329.80 | 324.34 |
| 3 | 478.55 | 474.81 | 473.86 | 474.40 | 473.83 |
| 4 | 567.69 | 555.22 | 555.00 | 555.10 | 555.03 |
| 5 | 708.29 | 702.80 | 670.48 | 687.05 | 663.68 |
| 6 | 851.54 | 848.68 | 812.16 | 817.12 | 797.27 |

**Table 4.8** Percent errors for the modes for each model using the spring stiffnesses of the full interface RBAR case

| Mode # | Full interface RBAR (%) | Full interface RBE3 (%) | Reduced interface RBAR (%) | Reduced interface RBE3 (%) |
|---|---|---|---|---|
| 1 | 0.60 | −4.30 | −1.78 | −5.28 |
| 2 | 0.37 | −1.76 | −0.58 | −2.23 |
| 3 | −0.78 | −0.98 | −0.87 | −0.99 |
| 4 | −2.20 | −2.24 | −2.22 | −2.23 |
| 5 | −0.78 | −5.34 | −3.00 | −6.30 |
| 6 | −0.34 | −4.62 | −4.04 | −6.37 |

In comparison to the optimal models, the frequencies for Modes 3 and 4 did not change. However, for all other modes, the frequency errors increased significantly though not dramatically

# References

1. Abaqus analysis user's guide. Simulia, (2014)
2. Jewell, E., Allen, M.S., Lacayo, R.: Predicting damping of a cantilever beam with a bolted joint using quasi-static modal analysis. In: Presented at the Proceedings of the ASME 2017 International Design Engineering Technical Conference & 13th International Conference on Multibody Systems, Nonlinear Dynamics, and Control IDETC/MSNDC 2017, (2017)
3. Segalman, D.J.: A four-parameter Iwan model for lap-type joints. J. Appl. Mech. **72**(5), 752–760 (2005)
4. Feldman, M.: Non-linear system vibration analysis using Hilbert transform–I. Free vibration analysis method 'Freevib'. Mech. Syst. Signal Process. **8**(2), 119–127 (1994)
5. Festjens, H., Chevallier, G., Dion, J.-L.: A numerical quasi-static method for the identification of frictional dissipation in bolted joints. In: Presented at the ASME 2012 International Design Engineering Technical Conferences and Computers and Information in Engineering Conference, IDETC/CIE 2012, August 12, 2012–August 12, 2012, 2012, vol. 1, pp. 353–358
6. Lacayo, R.M., Allen, M.S.: Updating structural models containing nonlinear Iwan joints using quasi-static modal analysis. Mech. Syst. Signal Process. **2017**, (2017)
7. Singh, A. et al.: Experimental characterization of a new benchmark structure for prediction of damping nonlinearity. In: Presented at the 36th International Modal Analysis Conference (IMAC XXXVI), Orlando, Florida (2018)
8. Kuether, R.J., Coffin, P.B., Brink, A.R.: On Hurty/Craig-Bampton substructuring with interface reduction on contacting surfaces. In: International Design Engineering Technical Conferences, Cleveland, Ohio (2017)
9. Craig, R.R.J., Bampton, M.C.C.: Coupling of substructures for dynamic analysis. AIAA J. **6**(7), 1313–1319 (1968)
10. Krattiger, D., et al.: Interface reduction for Hurty/Craig-Bampton substructured models: review and improvement. Mech. Syst. Signal Process. **114**, 579–603 (2017)
11. Sierra/SD – Theory manual. Sandia National Laboratories, Albuquerque, NM (2018)
12. Segalman, D.J., et al.: Handbook on Dynamics of Jointed Structures, vol. 87185. Sandia National Laboratories, Albuquerque, NM (2009)
13. Deaner, B.: Modeling the Nonlinear Damping of Jointed Structures Using Modal Models. University of Wisconsin-Madison, Madison, WI (2013)
14. Fronk, M. et al.: Inverse methods for characterization of contact areas in mechanical systems. In: Presented at the 36th International Modal Analysis Conference (IMAC XXXVI) (2018)